Three-dimensional ring vortex solitons and their stabilities in Bose-Einstein condensates under magnetic confinement

Ji Li,[1] Deng-Shan Wang,[2] Zhi-Yong Wu,[1,3] Yan-Mei Yu,[1,*] and Wu-Ming Liu[1]

[1]*Beijing National Laboratory for Condensed Matter Physics, Institute of Physics, Chinese Academy of Sciences, Beijing 100190, China*

[2]*School of Science, Beijing Information Science and Technology University, Beijing 100192, China*

[3]*Department of Applied Physics, Yanshan University, Qinhuangdao 066004, China*

(Received 17 July 2012; published 22 August 2012)

A three-dimensional study of the ring vortex solitons is conducted for both attractive and repulsive Bose-Einstein condensates subject to harmonic potential confinement. A family of stationary ring vortex solitons, which is defined by the radial excitation number and the winding number of the intrinsic vorticity, are obtained numerically for a given atomic interaction strength. We find that stabilities of the ground and radially excited states of the ring vortex soliton are dependent on the winding number differently. The ground state of the ring vortex soliton with the large winding number is unstable dynamically against random perturbation. The radially excited state of the ring vortex soliton with large winding number corresponds to the increased collapse threshold and therefore can be made stable for sufficiently small atomic interaction strengths. The ground and radially excited states also demonstrate different dynamic evolutions under large atomic interaction strengths. The former exhibits simultaneous symmetric splitting in the transverse plane, while the latter displays periodic expand-merge cycles in the longitudinal direction.

DOI: 10.1103/PhysRevA.86.023628 PACS number(s): 03.75.Lm, 05.45.Yv

I. INTRODUCTION

The realization of Bose-Einstein condensates (BECs) in dilute quantum gases has drawn a great deal of interest in vortices [1,2]. Recently, considerable effort has been aimed at the prediction of settings supporting stable multidimensional solitons with intrinsic vorticity. One such structure is the ring vortex soliton, where a soliton loops back on itself to form a ring and the phase of the wave function winds through an integer multiple of 2π radians around the vortex line. Such a ring vortex soliton can be defined by the quantum number set (n,S), where n is the radial excitation number, equal to the number of the rings, and S is the winding number of the intrinsic vorticity. One example of the ring vortex soliton, called "ring-profile solitary waves," has been studied in the context of optics [3,4]. Another example of the ring vortex soliton, called "vortex tori," has also been predicted in a three-dimensional (3D) cubic-quintic Ginzburg-Landau equation [5,6]. The ring dark soliton is first introduced in the repulsive BECs [7]. In a recent binary BEC experiment, ring bright solitons are also observed [8,9], which is studied further in theoretical works [10].

The most simple structure of the ring vortex soliton is of one ring in the radial direction, i.e., $n = 1$, which can be regarded as the radial ground state, and here we call it a single ring vortex soliton (SRVS). The bright vortex soliton created in the attractive and dipolar BECs [11–16] can be regarded as one typical example of SRVS. As we know, the atomic interaction in BECs can be controlled by the Feshbach resonance technique [17–19] to change the strength and sign of the interaction. Therefore, there is great interest in investigating the properties of the vortex soliton under the nonlinearity of the atomic interaction. It is predicted that SRVS is stable under the 3D harmonic trapping potential for sufficiently small interaction strengths [11,12,20], while for large interaction strengths the dynamic instability phenomena, such as split-merge cycles of particles [11,14,21] and intertwining of doubly quantized vortices [22–24], occur in the unstable regime.

An infinite sequence of radially excited stationary states of the ring vortex have been predicted by the Gross-Pitaevskii equation (GPE) in two dimensions (2D) and the sphere shell in three dimensions (3D) [25,26]. The radial excited state is of multiple concentric density-wave rings, i.e., $n \geqslant 2$, and here we call it the multiple ring vortex soliton (MRVS). The one-dimensional (1D) and 2D solutions of the MRVS are also proposed for a specific, spatially modulated nonlinearity [27–29]. In experiments, the ringlike excitations have been observed in the hyperfine states $|F = 1, m_f = -1\rangle$ and $|F = 2, m_f = +1\rangle$ of ^{87}Rb under a rotating cylindrical magnetic trap [8]. In $|\pm 1\rangle$ spinor ^{87}Rb BECs, more ringlike excitation modes have also been yielded under cylindrical magnetic confinement [9]. In theoretical simulations, a family of 3D gap solitons having multiple rings has been reproduced, as supported by 1D optical lattices [30].

In addition to the intrinsic vorticity, the MRVS has an additional excitation freedom, corresponding to an infinite number of nodes of the wave function in the radial direction. The early linear stability analytical results [25,26] have shown that, despite the radial excitation, the 2D (or 3D in the sphere shell) MRVS can be stable in the harmonic confinement below a threshold of the interaction strength. For large interaction strengths, the MRVS states are susceptible to collapse. When the instability times are much larger than the time scale $2\pi/\omega$, where ω is the harmonic trap frequency, it is said to be experimentally stable for small interaction strengths [25,26]. However, in a recent 3D study, it is found that the MRVS with $n = 2$ is unstable against quadrupole perturbations [30]. This implies that the radial excitation of MRVS could display more rich stability properties if subjected to 3D geometry.

*ymyu@iphy.ac.cn

This motivates us to investigate the stability of the MRVS in 3D space. Besides, considering the cylindrical magnetic confinement in the related experiments [8,9], the full 3D equation is necessary to study the ring vortex solitons.

In this paper, the 3D ring vortex solitons are constructed within the framework of GPE at the cylindrical coordinate for both attractive and repulsive BECs. The stabilities of SRVS and MRVS depend on S differently. The SRVS with $S = 1$ has better stability, i.e., large g_c, a threshold of the atomic interaction strength below which the ring vortex state is robustly stable against random perturbation, while the SRVS with $S \geqslant 2$ corresponds to the greatly decreased g_c and therefore has poor stability. On the contrary, the MRVS with large S has better stability, especially when the radial excitation is high. No or a very small stable regime is found for the MRVS with $S = 1$. The differences between the ground and radially excited states of the ring vortex soliton are further demonstrated in the dynamically unstable evolution. The SRVS shows the simultaneous symmetric splitting in the transverse plane, while the MRVS shows the periodic expand-merge cycles in the longitudinal direction before collapse. Such dynamic instability occurs at a time scale of about several seconds, being longer than $2\pi/\omega$, proving their good experimental stability.

The paper is outlined as follows. We first give a family of ring vortex solitons by using the Newton continuation method in Sec. II. Next, the stability properties of the ring vortex solitons are analyzed by using linear stability analysis in Sec. III, which is followed by the direct numerical simulations of the perturbed ring vortex solitons in Sec. IV. Finally, we conclude the main results of the work in Sec. V.

II. THEORETICAL MODEL AND STATIONARY SOLUTIONS

We consider the BECs in an external harmonic trapping potential $V(r,z) = m(\omega_r^2 r^2 + \omega_z^2 z^2)/2$, where $r^2 = x^2 + y^2$, m is the atom mass, and ω_r and ω_z are the radial and axial trapping frequencies. The wave function ψ of the BECs satisfies the dimensionless GPE,

$$i\frac{\partial\psi}{\partial t} = -\frac{1}{2}\left[\frac{1}{r}\frac{\partial}{\partial r}\left(r\frac{\partial}{\partial r}\right) + \frac{1}{r^2}\frac{\partial^2}{\partial\theta^2} + \frac{\partial^2}{\partial z^2}\right]\psi + V(r,z)\psi + g|\psi|^2\psi + i\Omega\frac{\partial\psi}{\partial\theta}, \quad (1)$$

where θ is the azimuthal angle, $g = 4\pi N a_s/a_0$ is the interaction strength, as determined by the total number of particles N in the condensate, the s-scattering wavelength a_s, and the harmonic oscillator length $a_0 = \sqrt{\hbar/\omega m}$, and Ω is the rotation angular frequency. The dimensionless $V(r,z) = \frac{1}{2}(\gamma_r^2 r^2 + \gamma_z^2 z^2)$ with $\gamma_r = \frac{\omega_r}{\omega}$, $\gamma_z = \frac{\omega_z}{\omega}$, and $\omega = \min\{\omega_r,\omega_z\}$. Equation (1) is obtained by rescaling the length by a_0, the time by ω^{-1}, and the energy by $\hbar\omega$.

Assume the wave function is

$$\psi(r,z,\theta,t) = \phi(r,z)e^{iS\theta - i\mu t}, \quad (2)$$

where S is azimuthal quantum number, i.e., the intrinsic vorticity, and μ is the chemical potential. The function $\phi(r,z)$ satisfies the equation

$$-\frac{1}{2}\left[\frac{1}{r}\frac{\partial}{\partial r}\left(r\frac{\partial}{\partial r}\right) + \frac{\partial^2}{\partial z^2} - \frac{S^2}{r^2}\right]\phi + V(r,z)\phi - S\Omega\phi + g\phi^3 = \mu\phi, \quad (3)$$

with the boundary conditions of $\lim_{\substack{r\to 0\\ |z|\to 0}} \phi(r,z) = 0$ and $\lim_{\substack{r\to\infty\\ |z|\to\infty}} \phi(r,z) = 0$. The linear-limit solution of Eq. (3) is written as the scaled linear combinations of products of the wave functions of the harmonic oscillator [31],

$$\phi(r,z) = \frac{\gamma_r^{(S+1)/2}\gamma_z^{1/4}}{\sqrt{\pi C_n^S}\pi^{1/4}} r^S \hat{L}_n^S(\gamma_r r^2)e^{-\frac{1}{2}(\gamma_r r^2 + \gamma_z z^2)}, \quad (4)$$

where $C_n^S = \prod_{j=1}^{S}(n+j)$, $\hat{L}_n^S$ is the generalized-Laguerre polynomials, and n is the quantum number in the r direction (the quantum number in the z direction has set to be zero). The chemical potential corresponding to Eqs. (3) and (4) is written as

$$\mu_{nS} = \gamma_r[2(n-1) + S + 1] - S\Omega + \tfrac{1}{2}\gamma_z. \quad (5)$$

The stationary soliton solutions can be obtained as numerical solutions of Eq. (3) using the Newton continuation method [32] with μ_{nS} input, starting with the linear-limit solutions, under the constraint that the normalization of the wave function $\tilde{N}$ and the energy E are conserved with numerical iteration time,

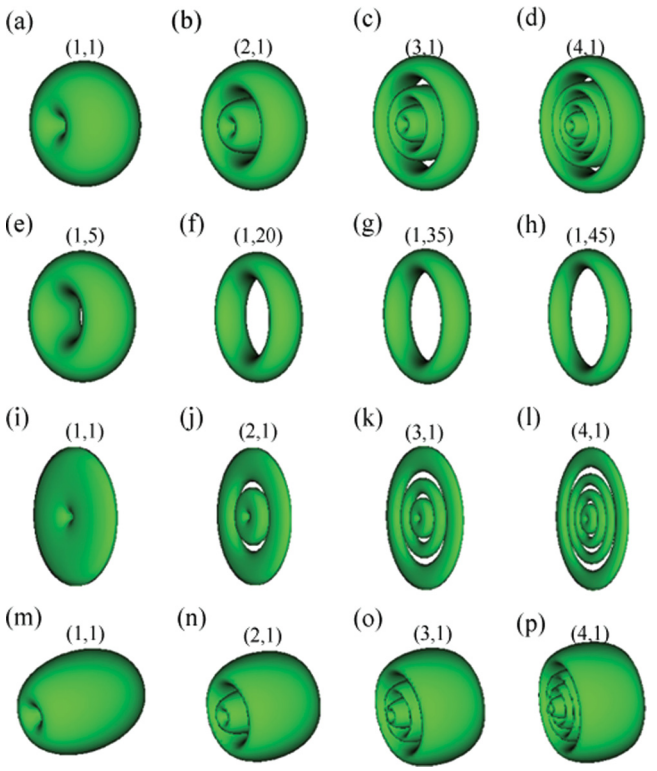

FIG. 1. (Color online) The 3D ring vortex solitons with different quantum-number sets (n,S) found numerically for attractive BECs, as visualized by the isosurface of dimensionless density of the wave function in the isotropic (a)–(h), pancake-shaped (i)–(l), and cigar-shaped (m)–(p) harmonic traps, respectively.

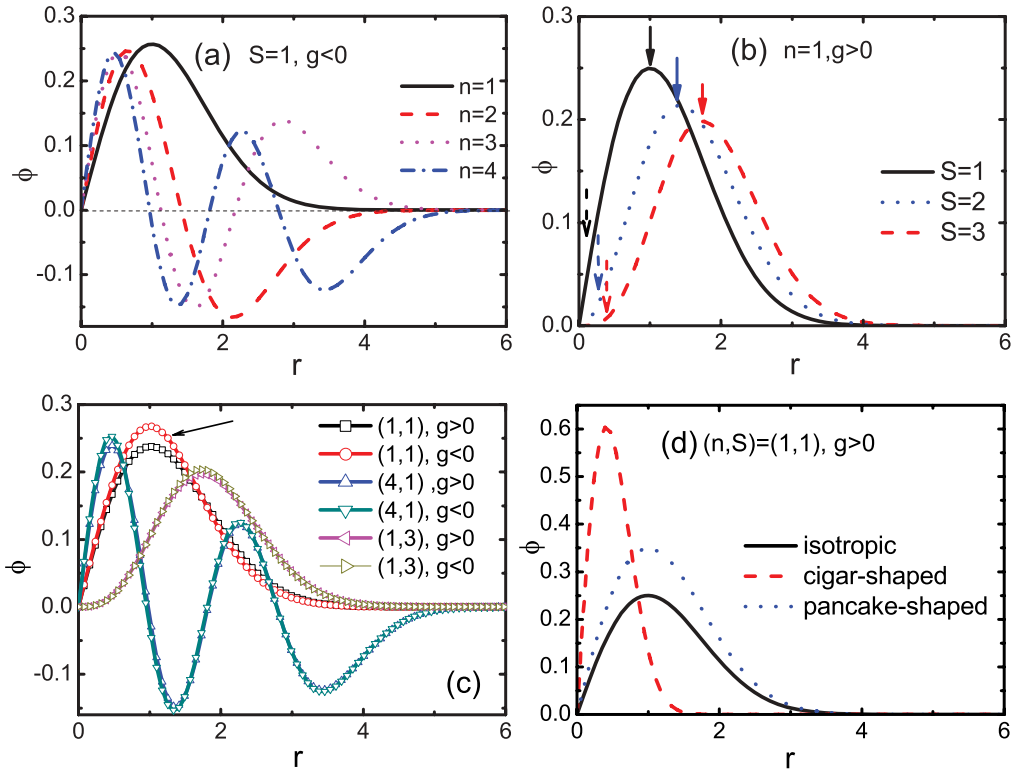

FIG. 2. (Color online) The radial density profile of the ring vortex solitons characterized by the quantum numbers (n,S) for the attractive $(g<0)$ or repulsive $(g>0)$ interactions under the isotropic harmonic potential in (a)–(c) and also the cigar-shaped and pancake-shaped harmonic potentials in (d).

where

$$\tilde{N}(\psi)=\int_{\mathbf{R}}|\psi(\mathbf{R},t)|^2 d\mathbf{R}=\tilde{N}(\psi_0)=1,\quad t\geqslant 0, \tag{6}$$

and the energy

$$\begin{aligned}E_{g,\Omega}(\psi)=&\int_{\mathbf{R}}\left[\frac{1}{2}|\psi(\mathbf{R},t)|^2+V(r,z)|\psi(\mathbf{R},t)|^2\right.\\&\left.+\frac{g}{2}|\psi(\mathbf{R},t)|^4-\Omega S\right]d\mathbf{R}\\\equiv& E_{g,\Omega}(\psi_0),\quad t\geqslant 0.\end{aligned} \tag{7}$$

Shown in Fig. 1 are various ring vortex solitons obtained in the case of the attractive interaction under different shaped harmonic potentials. For the isotropic harmonic potential of $\gamma_r=\gamma_z=1$, $g=-0.0083N$ refers to a ^{7}Li system both with $\omega_r=\omega_z=20\pi$ Hz, for the cigar-shaped harmonic potential of $\gamma_r=1.44$ and $\gamma_z=1$, $g=-0.0117N$ referring to ^{7}Li with $\omega_r=178$ Hz and $\omega_z=123$ Hz [33], and for the pancaked harmonic potential of $\gamma_r=1$ and $\gamma_z=20$, $g=-0.0083N$ referring to ^{7}Li with $\omega_r=20\pi$ Hz and $\omega_z=400\pi$ Hz [34]. In the case of isotropic harmonic potential, we also study the ring vortex solitons for the repulsive interactions, where $g=0.0188N$ refers to ^{87}Rb BECs with $\omega_r=\omega_z=20\pi$ Hz. In this work, $\Omega=0.7$ is fixed, except that is mentioned specifically. The vortex solitons obtained for the repulsive interactions (not shown here for the sake of brevity) resemble those shown in Fig. 1 for the attractive interaction.

The ring vortex solitons are further illustrated according to the radial profile of the wave function. Figure 2(a) shows that the influence of the quantum number n on the ring vortex solitons, i.e., the radially excited level is increasing with n, corresponding to more nodes of the wave function in the radial direction. Figure 2(b) shows the influence of the quantum number S on the ring vortex solitons. The ring vortex solitons

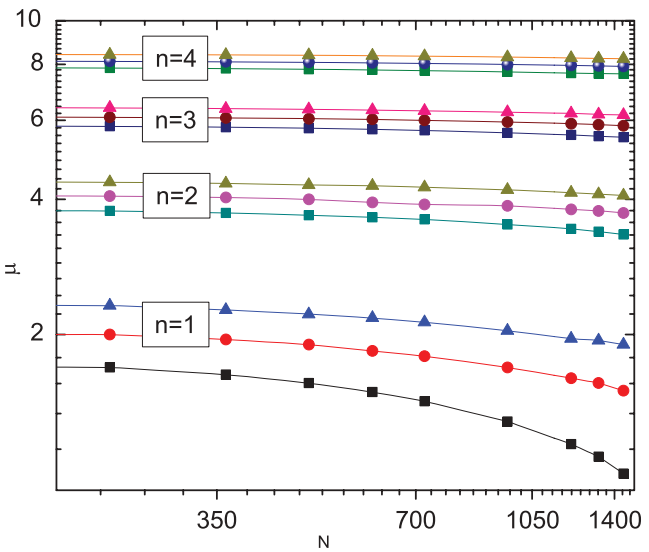

FIG. 3. (Color online) The $\mu(N)$ curves of the ring vortex solitons of $n=1,2,3,4$ with $S=1$ (square), $S=2$ (circle), and $S=3$ (triangular), as calculated with $\gamma_r=\gamma_z=1$ and $g=-0.0083N$, and $\Omega=0.7$, referring the ^{7}Li condensate under the isotropic harmonic potential with $\omega_r=\omega_z=20\pi$ Hz.

with the larger S demonstrate the deeper depletion of density at the core area (denoted by dashed arrows) and the lower density peak (denoted by solid arrows). Figure 2(c) shows the influence of the sign of the interaction nonlinearity on the shape of the ring vortex solitons for a given interaction strength. The density of the wave function at the first peak [denoted by the arrow in Fig. 2(c)] in the case of the attractive interaction is higher a little than that in the case of the repulsive interaction. Such a difference is the most prominent in the case of $(n,S) = (1,1)$ but is weak in the cases of large n or large S. Figure 2(d) illustrates variation of the radial profile of the ring vortex solitons under the different shaped harmonic potentials.

Shown in Fig. 3 is the $\mu(N)$ curves of the ring vortex solitons. For a given N, as compared to the SRVS family with $n = 1$, the MRVS families with $n = 2, 3, 4, \ldots$ are of increasing μ. Within a SRVS or MRVS family, μ is increasing with S. Each data shown in Fig. 3 corresponds to a convergent stationary state, which is further investigated for the stability and dynamic evolution.

III. STABILITY ANALYSIS

The stability of the ring vortex solitons is analyzed using the linear stability analysis. The wave function that deviates slightly from the stationary solutions is constructed as

$$\psi = [\phi(r,z) + ue^{iEt} + w^* e^{-iE^*t}]e^{iS\theta - i\mu t}, \qquad (8)$$

where $|u|, |w| \ll 1$ are eigenmodes. Substituting Eq. (8) into Eq. (1) gives

$$\begin{pmatrix} L & -g\phi^2 \\ g\phi^2 & -L \end{pmatrix} \begin{pmatrix} u \\ w \end{pmatrix} = E \begin{pmatrix} u \\ w \end{pmatrix}, \qquad (9)$$

where $L \equiv (\partial_{rr} + \frac{1}{r}\partial_r + \partial_{zz} - \frac{S^2}{r^2})/2 - V(r,z) - 2g\phi^2 + S\Omega + \mu$, and E is the eigenvalue related to u and w, which is obtained by diagonalization of Eq. (9) under the boundary conditions demanding that $u(r,z), w(r,z) \to 0$ at $r, |z| \to \infty$ and $r, |z| \to 0$. Applying Eq. (9), we analyze the ring vortex solitons of different radial excited states, not only the SRVS, i.e., $n = 1$, but also the MRVS, from the first radially excited state, i.e., $n = 2$, to the higher radially excited states.

Figure 4(a) shows the real and imaginary parts of eigenvalues of the SRVS obtained for a given interaction strength in an isotropic harmonic potential. When $S = 1$, all eigenvalues are real, indicating that the corresponding state is stable. When $S \geqslant 2$, complex eigenvalues emerge, indicating that the corresponding states are dynamically unstable. The inverse of the imaginary part of the complex eigenvalue, Im E, gives the time scale of such a dynamic instability. As shown in Figs. 4(a) and 4(b), it is found that Im E decreases with S, which indicates that the ring vortex soliton with the larger intrinsic vorticity is of the longer lifetime before collapse, i.e., the better experimental stability.

Moreover, Figs. 4(c) and 4(d) show the g dependence of Im E obtained for the SRVS with different S. The eigenvalues become complex above the critical interaction strength g_c, showing the onset of dynamic instability. The g_c value is dependent on S. For example, our results show that g_c is around -11 when $S = 1$ but decreases to -1.5 and -2 when $S = 5$ and 20 in the case of the attractive interaction. The corresponding value of g_c becomes a little larger in the case of the repulsive

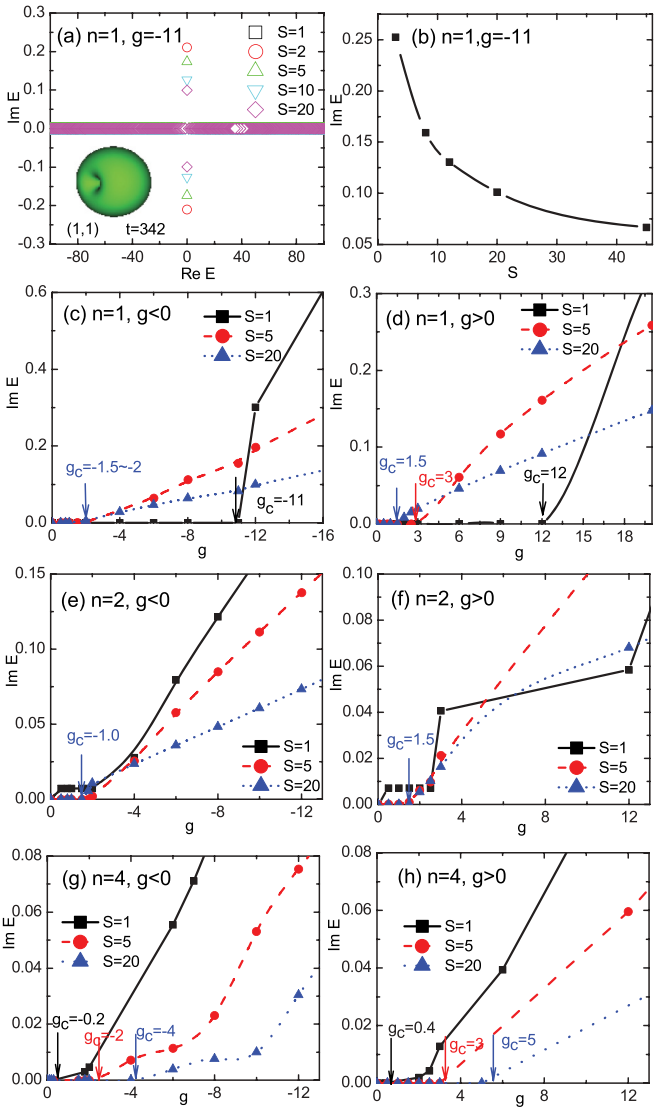

FIG. 4. (Color online) The imaginary part in the energy spectrums (Im E) of the stability analysis, (a),(b): Im E vs S obtained for SRVS under a given attractive interaction $g = -11$. The inset in (a) displays a robust SRVS wit $S = 1$ at dimensionless time $t = 342$ against noise perturbation, and Im E vs g obtained for SRVS [(c),(d)] and MRVS of $n = 2$ [(e) and (h)] and $n = 4$ [(g),(h)] with different S.

interaction, being around 12, 3, or 1.5 for the SRVS with $S = 1$, 5, and 20, respectively. The case of the SRVS, i.e., the general ring vortex soliton without radial excitation, has been studied previously [11,14,20]. It was found that for sufficiently weak interaction strength the SRVS with $S = 1$ is stable, while for $S \geqslant 2$ the SRVS is unstable to quadrupole oscillations. For instability times much longer than the time scale $2\pi/\omega$ of the BECs, the SRVS with $S \geqslant 2$ is said to be experimentally stable for small interaction strength. Our results shown in Figs. 4(a)–4(c) are consistent with the previous study for the general ring soliton without radial excitation [11,14,20].

Figures 4(e) and 4(f) show the curve of Im E vs g obtained for the MRVS of $n = 2$, i.e., the first excited state. The stability of the ring vortex soliton of the first radial excited state has been studied based on the 2D solutions [25], which shows that the first radial excited state with $S = 1$ is stable for the

sufficiently small interaction strength below a critical value. In our 3D study, for $S = 1$, no stable regime is found for the first excited state. This result means that the 3D MRVS of the first excited state with $S = 1$ could be different from its counterpart in 2D. The critical dimensionality for the GPE is 2D. Further, we find that for large S, the 3D MRVS can be made stable. For example, we give two Im E vs g curves obtained for MRVS with $S = 5$ and $S = 20$ in Figs. 4(e) and 4(f), where the stable regime, though being very small, is found up to $g_c = -1.0$ in the case of the attractive interactions and $g_c = 1.5$ in the case of the repulsive interactions. Such results indicate that the stability of the MRVS is dependent on the intrinsic vorticity. The MRVS with large S is expected to be stable.

Shown in Figs. 4(g) and 4(h) are results for the MRVS of $n = 4$. The S dependence on the stability becomes more prominent when the MRVS is of the higher radial excitation. The stable region, though being very small, below $g_c = -0.2$ and $g_c = 0.4$, is found for the $n = 4$ MRVS, with $S = 1$ under the attractive and repulsive interactions. The stable region increases for large S. When $S = 5$, the stable regions are up to $g_c = -2$ and $g_c = 3$ in the cases of the attractive and repulsive interactions, respectively. Furthermore, when $S = 20$, the stable regions increase up to $g_c = -4$ and $g_c = 5$ in the cases of the attractive and repulsive interactions, respectively. Through comparing two cases of $n = 2$ [Figs. 4(e) and 4(f)] and $n = 4$ [Figs. 4(g) and 4(h)], we can find that the intrinsic vorticity tends to improve the stability of the MRVS, and such an effect becomes more significant when the radial excitation of MRVS is high. The MRVS of large S has a prominent stable region.

The linear stability analytic results for the S dependence of the MRVS stability is further confirmed by the directed simulation based on Eq. (1). Corresponding to Fig. 4(e), Figs. 5(a) and 5(b) prove that the radially first-excited state of MRVS of $n = 2$ is unstable against random perturbation when $S = 1$ but becomes stable when S is large, such as $S = 5$, under a small g. Next, corresponding to Fig. 4(g), Figs. 5(c)–5(e) show the stable MRVS of $n = 4$ with different S values under the given interaction strength below an increasingly large g_c.

IV. DYNAMIC EVOLUTION

The ring vortex solitons are unstable against dynamic instability when the interaction strength is larger than g_c. Such dynamic instability is simulated through numerically integrating Eq. (1) using the time-splitting-spectral technique [35]. In our simulation, the stationary solutions of the ring vortex solitons are used as initial states after adding a random perturbation of a 1% relative amplitude of density.

We first simulate the dynamic evolution of the SRVS. As shown in Fig. 6, the SRVS evolves into polygonal rings, then splits into small fragments, and finally collapses. The multiple symmetry is revealed during such evolution. As S increases, we obtain the two-, three-, four-, five-, six-, seven-, and eightfold symmetry, as shown in Figs. 6 and 7. As seen in the phase profile of the wave function, the multiply quantized vorticity splits into many singly quantized vortices. Such a singly quantized vortex cannot be seen in the density plot, and hence they are called hidden (or ghost) vortices [36,37]. The singly quantized vortices are self-organized into the regular lattice, contributing to the symmetry in splitting. Such symmetry in instability

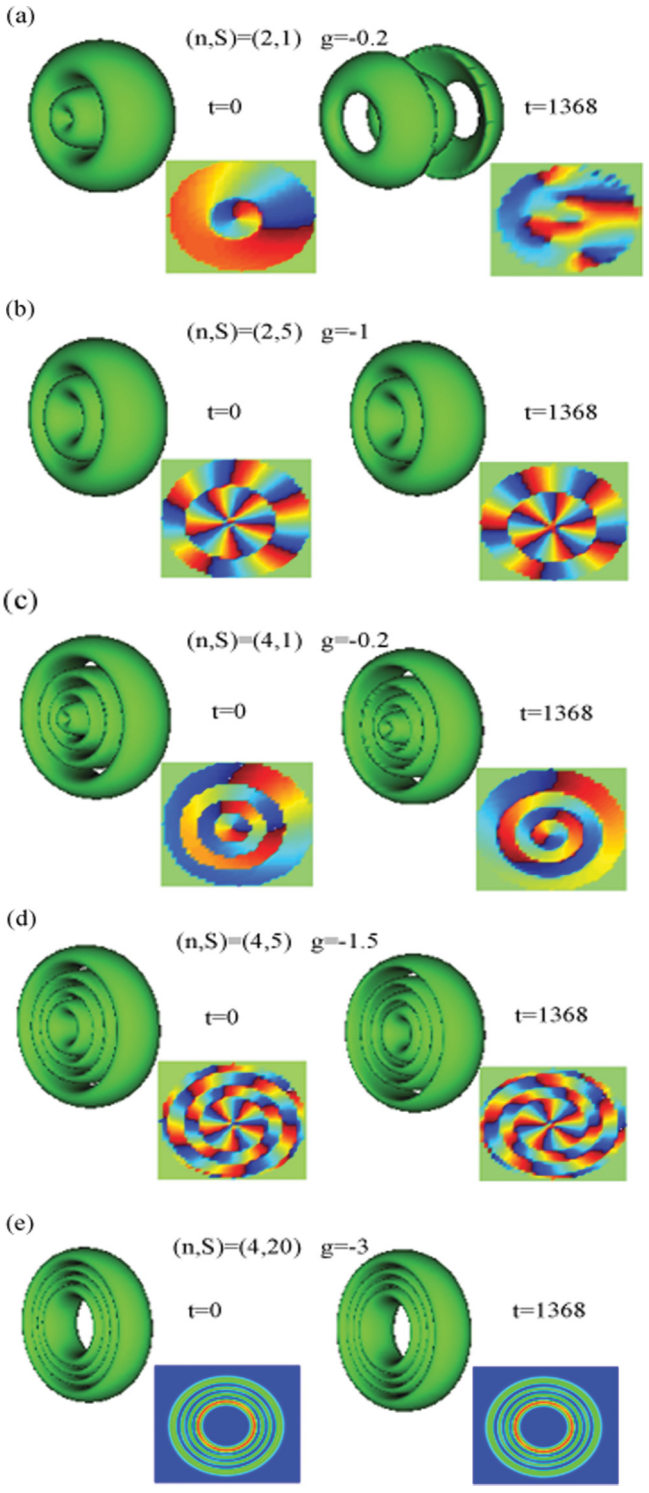

FIG. 5. (Color online) The dynamic evolution of the MRVS in unstable and stable regions in Figs. 4(e) and 4(f), where (a) is dynamically unstable and (b)–(e) are dynamically stable states which are consistent with linear stability analysis. Referring to a ^{7}Li system confined by $\omega_r = \omega_z = 20\pi$ Hz, the size is about 120 μm and the real time $t' = 0.0159t$ sec, and $t = 0$ corresponds to the initial state of a 1% random perturbation in density.

can be regarded as simultaneous, because the random initial perturbation we add is of no azimuthal mode. The multiple symmetric splitting phenomena has been demonstrated for

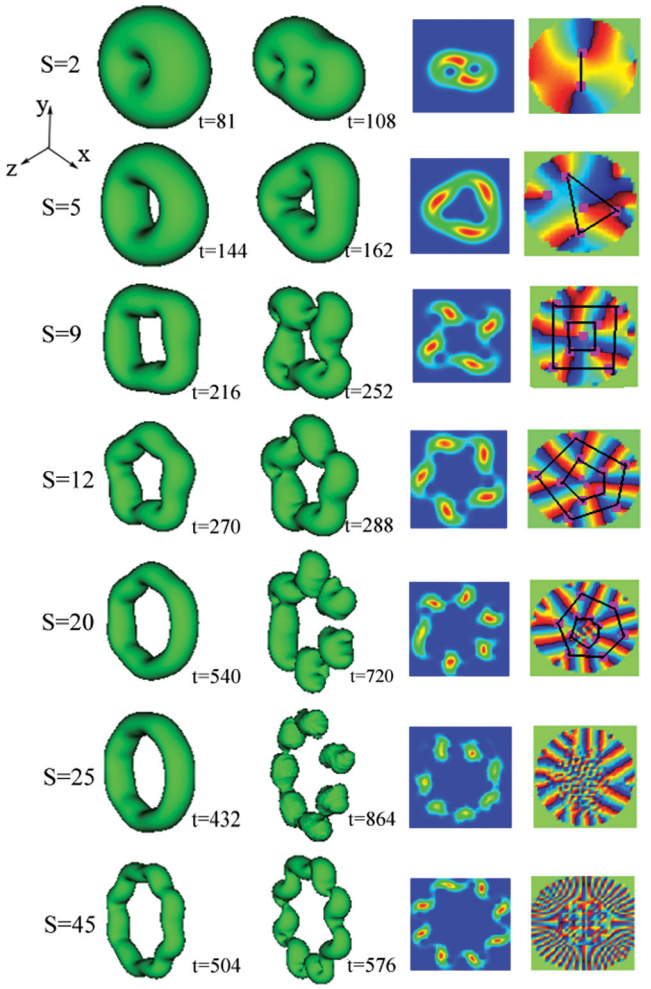

FIG. 6. (Color online) Noise-induced splitting of the ring vortex solitons of different S at dimensionless time t, and the corresponding density and phase (the third and forth columns) plots in the x-y plane. To translate the results into the experiment-related units, we assume a ^{7}Li condensate containing about 1500 atoms in an isotropic harmonic potential with $\omega_r = \omega_z = 20\pi$ Hz. The radii of the ring vortex solitons here are about 120 μm, decaying at the real time $t' = 0.0159t$ sec.

giant vortices [38–41]. The symmetry in splitting and the number of the fragments are considered to be equal to the added angular-momentum quantum number of the Bogoliubov excitation mode responsible for the splitting [38,41]. Ones find a total of three types of splitting patterns—twofold, threefold, and fourfold symmetries—when the initial perturbation is random noise in the density of the wave function [40,41]. Figures 6 and 7 indicate that there could be more types of symmetries in splitting of the ring vortex soliton. As a matter of fact, the number of symmetry can be manipulated by the interaction strength g. As shown in Fig. 8, the number in symmetry (or the number of the fragments) decreases with g in the case of the repulsive interaction and increases with g in the case of the attractive interaction.

Second, we simulate the dynamic evolution of the MRVS. As shown in Fig. 9, the MRVS demonstrates expand-merge cycles, then collapses. The similar phenomenon, expand-shrink cycles occurring in the transverse direction, was predicted for the dark SRVS [11,14,21]. As compared with the dark SRVS,

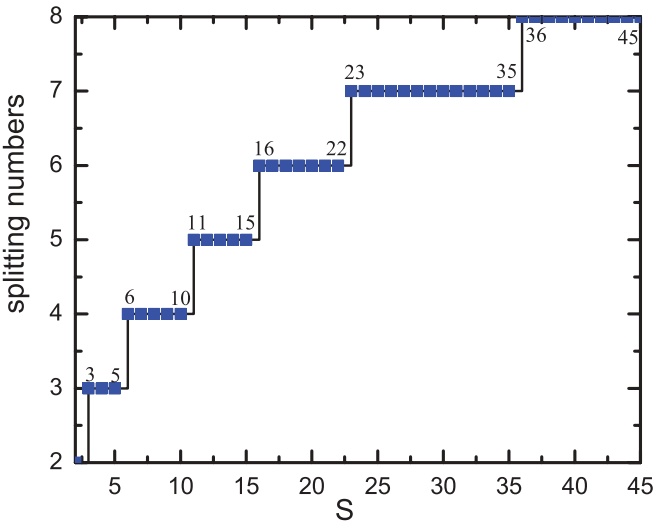

FIG. 7. (Color online) Noise-induced splitting of giant vortices. The splitting numbers as a function of different S for the attractive interaction are shown.

a principal difference is that the expand-merge cycles of the 3D MRVS occurs in the longitudinal direction. The condensate expands along the axial direction. The outer rings expand faster than the internal rings. At $t = 54$, the outmost ring splits into two pieces, and the internal rings expand but remain united. In contrast, the inmost ring shrinks, as seen in the density profile in the longitudinal plane shown in Fig. 9, middle row.

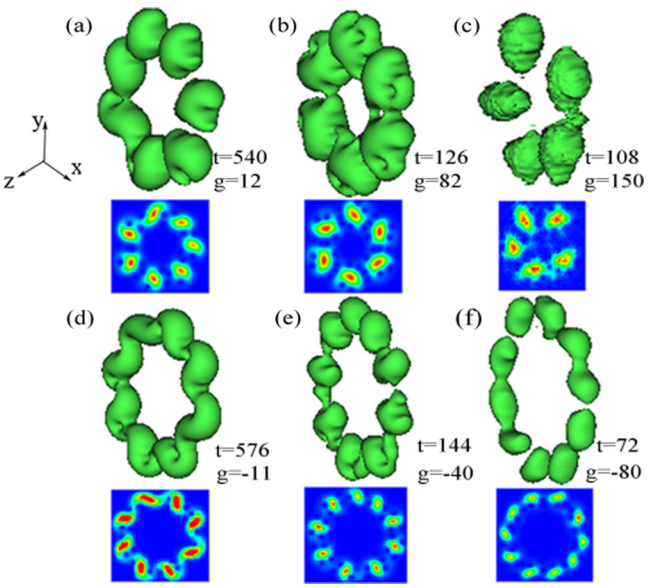

FIG. 8. (Color online) Noise-induced splitting of the 3D vortex solitons of large vorticity in (a)–(c) with $S = 25$ for the repulsive interaction and (d)–(f) with $S = 45$ for the attractive interaction. To translate the results into the experiment-related units, we assume the ^{87}Rb condensate containing about 640 (a), 4360 (b), and 8000 (c) atoms and the ^{7}Li condensate containing 1325 (d), 4820 (e), and 9638 (f) atoms in a isotropic harmonic potential with $\omega_r = \omega_z = 20\pi$ Hz. The radii of the ring vortex solitons here are about 31 μm for (a)–(c) and 120 μm, being snapshots at the real time $t' = 0.0159t$ sec.

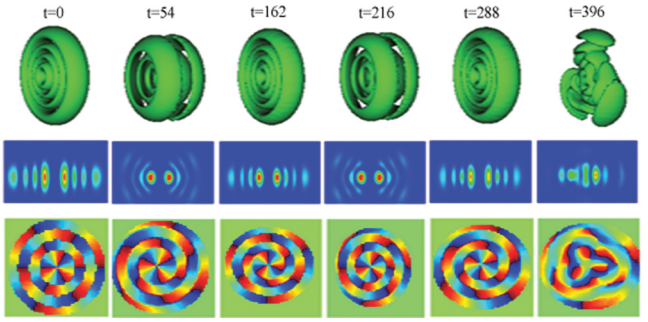

FIG. 9. (Color online) Noise-induced splitting of a vortex soliton of $(n,S) = (4,3)$ at the dimensionless time t and the corresponding density plot in the x-z plane (middle row) and phase plot in the x-y plane (lower row). To translate the results into experiment-related units, we assume a ^{7}Li condensate containing about 1500 atoms in an isotropic harmonic potential with $\omega_r = \omega_z = 20\pi$ Hz. The radii of the ring vortex solitons here are about 83.68 μm, decaying at the real time $t' = 0.0159t$ sec.

The expanded condensates and pieces subsequently unite to restore the original shape at $t = 162$. Such cycles repeat two times, then collapse finally. The expand-merge cycles reflect the expansion in the axial direction and the oscillation in the radial direction of the density of the wave function. In addition, during the dynamic evolution of the MRVS, as seen in the phase profile of the wave function in the transverse plane shown in Fig. 9, lower row, the multiply quantized vorticity is maintained well during the expand-shrink cycles. No vortex splitting is observed until the final collapse, which indicates that for the MRVS, the instability of the multiple radial waves prevails over the azimuthal instability. The similar expand-merge evolutions are demonstrated in the case of the repulsive interaction, where the cycles repeat three times before collapse, indicating the longer lifetime.

We also simulate the dynamic instability under the pancake-shaped and cigar-shaped harmonic potentials. The expand-merge cycle occurring for the isotropic harmonic potential is suppressed under the pancake confinement potential. Under the cigar-shaped harmonic potential, being elongated in the axial direction, the MRVS does not demonstrate expand-merge cycles either. Besides, another interesting dynamics phenomenon, intertwining of vortices in the cigar-shaped BECs [22–24], is also not observed in our simulations.

The present work is conducted under the rotating GPE frame, which facilitates the future further study that considers the possible dependence of the form and properties of the ring vortex soliton on the rotation angular frequency. The parameter $\Omega = 0.7$ used for Figs. 1–9 is chosen arbitrarily, referring to the rotating BEC experiment condition [42,43]. However, the results shown in Figs. 1–9 are of general interest, and the stable ring vortex solitons do not necessarily rely on such a specific Ω value, as found in our additional calculations with other Ω values. For example, the dimensionless density profiles of two kinds of stable stationary ring vortex solitons, the SRVS with $S = 1$ and the MRVS of $n = 4$ with $S = 20$ subject to the sufficient small interaction strength $g = g_c$, obtained for different Ω values overlap together, as shown in Figs. 10(a) and 10(b). The results indicate that the form of such ring vortex solitons hardly changes with variations of Ω. On the other hand, for a sufficiently small interaction strength $g = g_c$, all Im E obtained for $\Omega = 0, 0.4, 0.75$, and 0.95 are equal to zero,

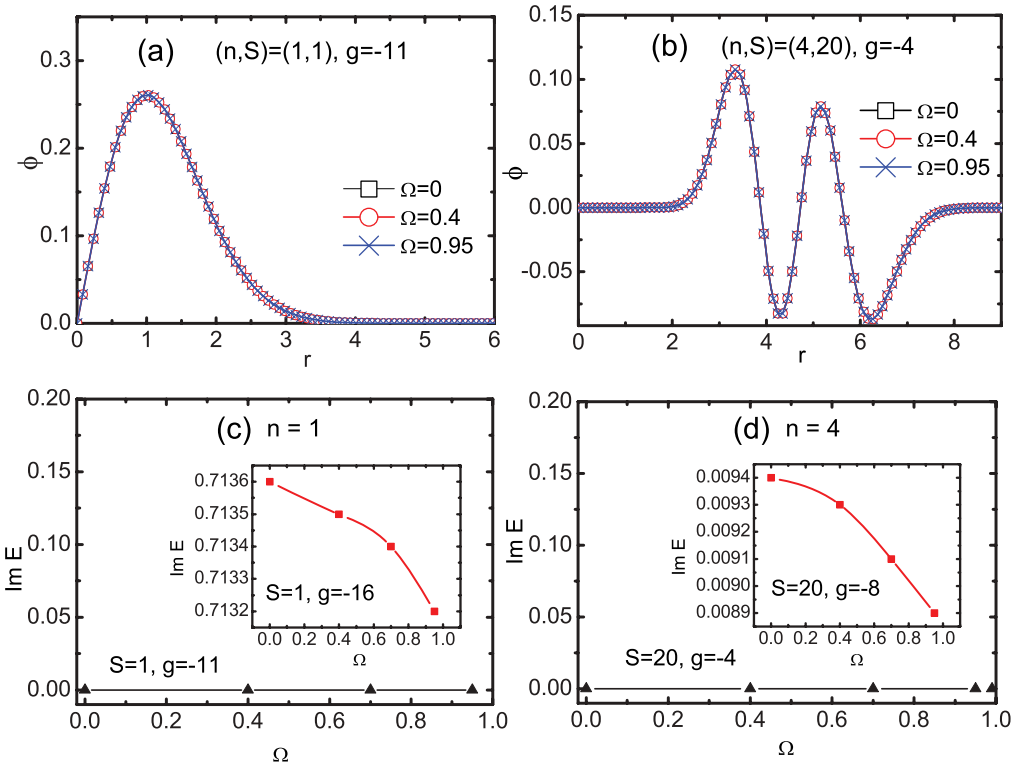

FIG. 10. (Color online) The ring vortex solitons obtained for different rotation frequencies Ω: (a) and (b) the radial density profile of the wave function, (c) and (d) the imaginary part in energy spectrums (Im E) of the stability analysis.

as shown in Figs. 10(c) and 10(d), which indicates that the SRVS with $S = 1$ and the MRVS with $S = 20$ maintain robust stability for different rotating frequencies. For an interaction strength larger than g_c, as shown in the insets in Figs. 10(c) and 10(d), Im E decreases with Ω, corresponding to longer lifetime in the dynamic unstable evolution; however, such influence is in the minor quantity range.

V. DISCUSSION AND CONCLUSIONS

With regard to the cylindrical magnetic confinement, we used a full 3D equation to investigate the stationary state, stability, and dynamic evolutions of the ring vortex solitons in the attractive and repulsive BECs. A family of stationary ring vortex solitons is obtained numerically by the Newton continuation method. The stability properties of the ring vortex solitons are predicted for a given interaction strength by using the linear stability analysis and confirmed further by direct simulation. The stabilities of the SRVS and MRVS depend on S differently. The SRVS with $S = 1$ corresponds to a large g_c, a threshold below which the solution is stable against random perturbation, while the SRVS with $S \geqslant 2$ corresponds to the greatly decreased g_c. The S dependence of the stability of the MRVS is contrary. The prominent stable regimes are found for the MRVS of $n = 4$ with large S, such as $S = 5$ and 20, while very small stable regimes are obtained for the MRVS of $n = 4$ with $S = 1$, and no stable regime is even found for MRVS of $n = 2$ with $S = 1$.

Therefore, we can expect the robust dynamic stability against random perturbation for the SRVS with $S = 1$ and the MRVS with large S when the atomic interaction strength is less than g_c. For the radial ground state of the ring vortex soliton, the values of g_c are around -11 and 12, as predicted for the SRVS with $S = 1$ under the attractive and repulsive interactions. For the radially excited state, the values of g_c are around -4 and 5, as predicted for the MRVS with $S = 20$ under the attractive and repulsive interactions. In our study, we consider a cylindrical magnetic trap with a harmonic frequency of $\omega_r = \omega_z = 20\pi$ Hz, which corresponds to the critical atom number of the stable ring vortex soliton being about 600∼1300 in the case of the radially ground state (where we refer to the ^{87}Rb system with $a_s = 51$ Å and $m = 1.44 \times 10^{-25}$ kg, the ^{7}Li system with $a_s = -79.35$ Å, and $m = 1.1702 \times 10^{-26}$ kg, respectively), and several hundreds in the case of the radially excited state. To decrease the magnetic harmonic frequency down to several Hertz, one can expect that the critical atom number increases to 10^3∼10^4. Our results suggest the possible conditions that the ring vortex soliton can be made stable against random perturbation.

On the other hand, our study also suggests some most unstable states of the ring vortex solitons, for example, the SRVS with $S \geqslant 2$ and the MRVS with $S = 1$. Our direct simulations show that the lifetime of the dynamic evolution can be several seconds before the final collapse, for example, the SRVS shown in Fig. 6 and the MRVS shown in Fig. 9 show that about 10^3 atoms can survive up to 1.5–8 sec if referring to a magnetic trapping potential with frequency $\omega = 20\pi$. Such time scales are far larger than the time scale $2\pi/\omega$ [25,26]. Therefore, the dynamic evolution results further suggest that the ring vortex solitons could be observed in experiments if subjected to an appropriate interaction strength. The differences between the ground and radially excited states of the ring vortex soliton are also reflected in the different evolutions before collapse. In the dynamically unstable regime subjected to the large atomic interaction, the SRVS demonstrates the simultaneous symmetric splitting in the transverse plane, while the MRVS exhibits the periodical expand-merge cycles in the longitudinal direction.

Rotation is one condition for generating vortices in BEC, and the rotation of a macroscopic quantum state often involves a dramatic change of its properties. For example, Ho showed that as the rotating frequency Ω is very close to radial frequency ω_r, the system reaches a quantum Hall regime where the density profile is a Gaussian in the xy plane and an inverted parabolic profile along the z direction [44]. Kartashov *et al.* investigated the guiding-center solitons in rotating period potentials and showed that the increase of Ω results in formation of a stable soliton, whose shape is almost identical to the initial state [45]. Sakaguchi and Malomed studied the gap solitons in rotating optical lattices and demonstrated that there is a critical rotating frequency Ω_c. The soliton state is stable for an indefinitely long time for $\Omega < \Omega_c$ but is unstable against decay into radiation waves for $\Omega > \Omega_c$ [46]. Jamaludin *et al.* studied the bright solitary waves of atomic BEC under rotation and showed that Ω has a considerable stabilizing effect on the system, significantly raising the critical threshold for collapse of the bright solitary waves [47]. Lashkin and Maucher *et al.* presented exact numerical solutions in the form of spatially localized 3D rotating multiple solitons in BEC confined by a parabolic trap and showed that the 3D azimuthal solutions exist as a continuous family parameterized by rotating frequency Ω [48,49]. In these works, the vortex comes from the rotation conditions and therefore depends on the rotation frequency somehow.

In the present work, the vortex is embedded in the input through imprinting a topological phase pattern onto the initial BEC wave function in terms of $e^{(iS\theta-\cdots)}$ in Eq. (2). In recent years, imprinting vortices in a BEC using topological phases has been done by many researchers [50,51]. Such initial wave functions are widely used for the study of singly, doubly, or multiply quantized vortices [11,22,52]. As bases of the present work, the exact stationary solutions of ring vortex solitons with topological phases have been proposed in the nonrotating [28] and rotating BEC framework [29]. It is shown that when the initial state is the exact stationary solutions with topological charge, the stability and the number of vortices are almost the same for both rotating and nonrotating BECs.

We obtain the stationary solutions with the topological charge with high numerical accuracy by the Newton continuation method in the present work. We imprint a topological phase pattern onto the input BEC and find many ring vortex solitons. Our results in the present work show that the form, stability, and dynamically unstable lifetimes of such ring vortex solitons almost do not change with variations of Ω. The reason is probably because the intrinsic vorticity is imprinted in a topological phase, not stemming from the rotation condition. In this present work, Ω only enters into the chemical potential of the wave function through the term $S\Omega$ in Eq. (5), and this term does not influence the dimensionless profile of the wave function of the ring vortex solitons. The effect caused by

such a term is also weak in the stability analysis and dynamic evolution of the ring vortex solitons.

Our results suggest possibilities for creation and observation of robust 3D ring vortex solitons in the cylindrical geometry under a magnetic harmonic trap. The two most stable ring vortex solitons, the SRVS with $S = 1$ and the MRVS of large S, show robust forms and stabilities for different rotation frequencies of the trap, which means that the stable ring vortex soliton can be made in either the rotating or the nonrotating BECs.

ACKNOWLEDGMENTS

This work was supported by NKBRSF of China (Grants No. 2012CB821305 and No. 2011CB921502) and NSFC (Grants No. 10974228 and No. 11001263).

[1] M. R. Matthews, B. P. Anderson, P. C. Haljan, D. S. Hall, C. E. Wieman, and E. A. Cornell, Phys. Rev. Lett. **83**, 2498 (1999).
[2] A. L. Fetter and A. A. Svidzinsky, J. Phys.: Condens. Matter **13**, R135 (2001).
[3] W. J. Firth and D. V. Skryabin, Phys. Rev. Lett **79**, 2450 (1997).
[4] A. Dreischuh, W. Fließer, I. Velchev, S. Dinev, and L. Windholz, Appl. Phys. B **62**, 139 (1996).
[5] D. Mihalache, D. Mazilu, F. Lederer, Y. V. Kartashov, L.-C. Crasovan, L. Torner, and B. A. Malomed, Phys. Rev. Lett. **97**, 073904 (2006).
[6] V. Skarka, N. B. Aleksić, H. Leblond, B. A. Malomed, and D. Mihalache, Phys. Rev. Lett. **105**, 213901 (2010).
[7] G. Theocharis, D. J. Frantzeskakis, P. G. Kevrekidis, B. A. Malomed, and Y. S. Kivshar, Phys. Rev. Lett. **90**, 120403 (2003).
[8] K. M. Mertes, J. W. Merrill, R. Carretero-González, D. J. Frantzeskakis, P. G. Kevrekidis, and D. S. Hall, Phys. Rev. Lett. **99**, 190402 (2007).
[9] M. Scherer, B. Lücke, G. Gebreyesus, O. Topic, F. Deuretzbacher, W. Ertmer, L. Santos, J. J. Arlt, and C. Klempt, Phys. Rev. Lett. **105**, 135302 (2010).
[10] K. J. H. Law, P. G. Kevrekidis, and L. S. Tuckerman, Phys. Rev. Lett. **105**, 160405 (2010).
[11] H. Saito and M. Ueda, Phys. Rev. Lett. **89**, 190402 (2002).
[12] H. Saito and M. Ueda, Phys. Rev. Lett. **90**, 040403 (2003).
[13] H. Saito and M. Ueda, Phys. Rev. A **69**, 013604 (2004).
[14] D. Mihalache, D. Mazilu, B. A. Malomed, and F. Lederer, Phys. Rev. A **73**, 043615 (2006).
[15] B. A. Malomed, F. Lederer, D. Mazilu, and D. Mihalache, Phys. Lett. A **361**, 336 (2007).
[16] Y. A. Zaliznyak and A. L. Yakimenko, Phys. Lett. A **372**, 2862 (2008).
[17] S. Inouye, M. R. Andrews, J. Stenger, H.-J. Miesner, D. M. Stamper-Kurn, and W. Ketterle, Nature (London) **392**, 151 (1998).
[18] P. G. Kevrekidis, G. Theocharis, D. J. Frantzeskakis, and B. A. Malomed, Phys. Rev. Lett. **90**, 230401 (2003).
[19] S. E. Pollack, D. Dries, M. Junker, Y. P. Chen, T. A. Corcovilos, and R. G. Hulet, Phys. Rev. Lett. **102**, 090402 (2009).
[20] H. Pu, C. K. Law, J. H. Eberly, and N. P. Bigelow, Phys. Rev. A **59**, 1533 (1999).
[21] L. Salasnich and B. A. Malomed, Phys. Rev. A **79**, 053620 (2009).
[22] M. Möttönen, T. Mizushima, T. Isoshima, M. M. Salomaa, and K. Machida, Phys. Rev. A **68**, 023611 (2003).
[23] A. M. Mateo and V. Delgado, Phys. Rev. Lett. **97**, 180409 (2006).
[24] J. A. M. Huhtamäki, M. Möttönen, T. Isoshima, V. Pietilä, and S. M. M. Virtanen, Phys. Rev. Lett. **97**, 110406 (2006).
[25] L. D. Carr and C. W. Clark, Phys. Rev. Lett. **97**, 010403 (2006).
[26] L. D. Carr and C. W. Clark, Phys. Rev. A **74**, 043613 (2006).
[27] Q. Tian, L. Wu, J. F. Zhang, B. A. Malomed, D. Mihalache, and W. M. Liu, Phys. Rev. E **83**, 016602 (2011).
[28] L. Wu, L. Li, J. F. Zhang, D. Mihalache, B. A. Malomed, and W. M. Liu, Phys. Rev. A **81**, 061805(R) (2010).
[29] D. S. Wang, S. W. Song, B. Xiong, and W. M. Liu, Phys. Rev. A **84**, 053607 (2011).
[30] A. Muñoz Mateo, V. Delgado, and B. A. Malomed, Phys. Rev. A **82**, 053606 (2010).
[31] W. Bao, H. Li, and J. Shen, SIAM J. Sci. Comput. **31**, 3685 (2009).
[32] W. Bao and W. Tang, J. Comput. Phys. **187**, 230 (2003).
[33] C. C. Bradley, C. A. Sackett, J. J. Tollett, and R. G. Hulet, Phys. Rev. Lett. **75**, 1687 (1995).
[34] D. Rychtarik, B. Engeser, H.-C. Nägerl, and R. Grimm, Phys. Rev. Lett. **92**, 173003 (2004).
[35] W. Bao and H. Wang, J. Comput. Phys. **217**, 612 (2006).
[36] M. Tsubota, K. Kasamatsu, and M. Ueda, Phys. Rev. A **65**, 023603 (2002).
[37] L. Wen, H. Xiong, and B. Wu, Phys. Rev. A **82**, 053627 (2010).
[38] Y. Kawaguchi and T. Ohmi, Phys. Rev. A **70**, 043610 (2004).
[39] M. Möttönen, V. Pietilä, and S. M. M. Virtanen, Phys. Rev. Lett. **99**, 250406 (2007).
[40] T. Isoshima, M. Okano, H. Yasuda, K. Kasa, J. A. M. Huhtamäki, M. Kumakura, and Y. Takahashi, Phys. Rev. Lett. **99**, 200403 (2007).
[41] P. Kuopanportti and M. Möttönen, Phys. Rev. A **81**, 033627 (2010).
[42] V. Bretin, S. Stock, Y. Seurin, and J. Dalibard, Phys. Rev. Lett. **92**, 050403 (2004).
[43] K. W. Madison, F. Chevy, V. Bretin, and J. Dalibard, Phys. Rev. Lett. **86**, 4443 (2001).
[44] T-L. Ho, Phys. Rev. Lett. **87**, 060403 (2001).
[45] Y. V. Kartashov, B. A. Malomed, and L. Torner, Phys. Rev. A **75**, 061602 (2007).
[46] H. Sakaguchi and B. A. Malomed, Phys. Rev. A **79**, 043606 (2009).
[47] N. A. Jamaludin, N. G. Parker, and A. M. Martin, Phys. Rev. A **77**, 051603 (2008).
[48] V. M. Lashkin, Phys. Rev. A **78**, 033603 (2008).
[49] F. Maucher, S. Skupin, M. Shen, and W. Krolikowski, Phys. Rev. A **81**, 063617 (2010).
[50] J. Denschlag, J. E. Simsarian, D. L. Feder, Charles W. Clark, L. A. Collins, J. Cubizolles, L. Deng, E. W. Hagley, K. Helmerson, W. P. Reinhardt, S. L. Rolston, B. I. Schneider, and W. D. Phillips, Science **287**, 97 (2000).
[51] A. E. Leanhardt, A. Görlitz, A. P. Chikkatur, D. Kielpinski, Y. Shin, D. E. Pritchard, and W. Ketterle, Phys. Rev. Lett. **89**, 190403 (2002).
[52] Y. Kawaguchi and T. Ohmi, Phys. Rev. A **70**, 043610 (2004).